Line Structure-Based Indoor and Outdoor Integration Using Backpacked and TLS Point Cloud Data

Chenglu Wen, *Senior Member, IEEE*, Xiaotian Sun, Shiwei Hou, Jinbin Tan, Yudi Dai, Cheng Wang, *Senior Member, IEEE*, and Jonathan Li, *Senior Member, IEEE*

***Abstract*— This letter presents a line structure-based method for integration of centimeter-level indoor backpacked scanning point clouds and millimeter-level outdoor terrestrial laser scanning point clouds. Using 3-D lines for registration, instead of matching points directly, can improve the robustness of the method and adapt to multisource point cloud data of different qualities. Considering the limited overlapping between indoor and outdoor scenes, line structures are extracted from overlapped wall areas that may be included in interior and exterior data. Here, a patch-based method labels a point cloud into wall, ceiling, floor categories, as well as assigning the candidate overlapping walls. Then, lines structures are extracted from the wall plane point cloud. Potential door and window line structures are detected and refined for point cloud registration. Last, an iterative closest point-based method is used to fine tune the registration results. Our results show that the proposed method effectively integrates a promising map of indoor and outdoor scenes.**

***Index Terms*— Indoor outdoor integration, line feature, point clouds, semantic labeling.**

I. Introduction

IN RECENT years, 3-D building models have received more and more attention. Current building modeling is generally achieved by modeling software or automated methods based on image/point cloud data. To better serve the needs of complete building modeling, indoor and outdoor 3-D scene data must be integrated. Because of the differences between indoor and outdoor environments, indoor and outdoor 3-D scene data are commonly acquired by different mapping devices, which create a demand to develop a method that integrates multisource indoor and outdoor data of different qualities. This integration problem is quite different from the registration of the same-source 3-D scene data [1].

Manuscript received April 17, 2018; revised June 5, 2018 and June 26, 2018; accepted July 12, 2018. This work was supported in part by the National Science Foundation of China under Grant 61771413 and in part by the Fundamental Research Funds for the Central Universities under Grant 20720170047. *(Corresponding author: Chenglu Wen.)*

C. Wen, X. Sun, S. Hou, J. Tan, Y. Dai, and C. Wang are with the Fujian Key Laboratory of Sensing and Computing for Smart City, School of Information Science and Engineering, Xiamen University, Xiamen 361005, China, and also with the Fujian Collaborative Innovation Center for Big Data Applications in Governments, Fuzhou 350003, China (e-mail: clwen@xmu.edu.cn).

J. Li is with the Fujian Key Laboratory of Sensing and Computing for Smart City, School of Information Science and Engineering, Xiamen University, Xiamen 361005, China, with the Fujian Collaborative Innovation Center for Big Data Applications in Governments, Fuzhou 350003, China, and also with the GeoSTARS Laboratory, Department of Geography and Environmental Management, University of Waterloo, Waterloo, ON, Canada (e-mail: junli@xmu.edu.cn).

Color versions of one or more of the figures in this letter are available online at http://ieeexplore.ieee.org.

Digital Object Identifier 10.1109/LGRS.2018.2856514

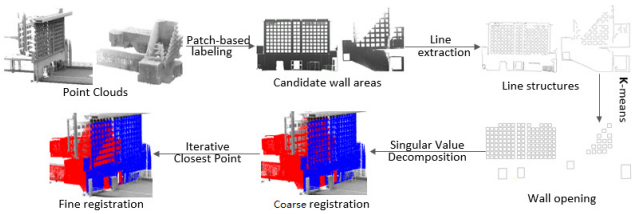

Fig. 1. Pipeline of the proposed method.

The key to matching indoor and outdoor data is to find the same structure that appears in both scenes. Windows and doors, which connect indoor and outdoor areas, are commonly used as matching structures. Many methods have been developed to integrate indoor and outdoor building data based on images. Koch *et al.* [2] proposed a method to align indoor and outdoor building models using 3-D line segments extracted from the image structure from motion (SFM) data [3]. To align the interior and exterior of a building, Cohen *et al.* [4] proposed using SFM models and images to generate correspondences, based on the windows between the two models.

Compared with images, point cloud data provide denser, more accurate feature information to register indoor and outdoor scenes. Mellado *et al.* [5] proposed super four-points congruent sets (4PCS) registration method based on the original 4PCS method [6]. Most current methods are suitable for same source point cloud registration. Because different devices and methods are commonly used to obtain indoor and outdoor point cloud data, the qualities (e.g., density, noise level, and accuracy) of the data are different. Meanwhile, the overlapping region of the indoor and outdoor data is usually very limited. These difficulties create a challenge for the integration of the indoor and outdoor data.

To integrate backpacked indoor data with terrestrial laser scanning (TLS) outdoor data, we propose an indoor–outdoor integration method based on 3-D line structures. (The pipeline is shown in Fig. 1.) To obtain a candidate wall area, patch-based point cloud semantic labeling is first performed. To ensure the registration between the different quality data, 3-D line structures are extracted directly from an overlapped point cloud for coarse registration. Final fine registration is achieved by an iterative closest point (ICP)-based method.

II. Indoor and Outdoor Data Acquisition

A. Backpacked Indoor 3-D Mobile Mapping

Based on our previous indoor backpacked laser scanning system [7] shown in Fig. 2(a), to acquire indoor point cloud data, we built an upgraded indoor backpacked laser scanning

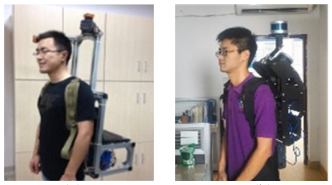

(a) (b)

Fig. 2. Backpacked indoor laser scanning system. (a) Single-beam backpacked system [7]. (b) Upgraded multibeam backpacked system [8].

system [8] as shown in Fig. 2(b), which consists of two calibrated 16-beam 3-D laser scanners (Velodyne VLP-16).

Indoor 3-D mapping was achieved by a light detection and ranging (LIDAR)-based simultaneous localization and mapping method. Based on the LIDAR odometry and mapping method [9], the feature points on sharp edges and planar surface patches were first extracted in each LIDAR data frame. Because each acquired frame included multiple individual lines, the smoothness of every point was evaluated through the spatial relationship with its surrounding points. Then these features were matched to reconstruct a 3-D point cloud map, as well as a trajectory. Loop closures were detected by the distance between the frames. If, for an extended period, two frames are discontinuous, and their spatial distance is less than a threshold, a possible closed loop is detected. Last, a general framework for graph optimization (G2O) framework [10] was adopted to optimize the map.

B. Outdoor Data Acquisition

With the assistance of the global positioning system/global navigation satellite system, there are many commercial survey systems available to acquire outdoor data, for example, the air/UAV-borne laser scanning system (ALS), vehicle-borne mobile laser scanning system (MLS), and TLS. The MLS and TLS are commonly used survey-level systems which provide up to 1 angular resolution and millimeter precision. In this letter, we acquired the outdoor scene data by a TLS device.

III. Line Structure-Based Indoor and Outdoor Integration

A. Patch-Based Point Cloud Semantic Labeling

Line extraction from a single plane yields better results than line extraction directly from the entire point cloud. Semantic labeling is first performed on the entire point cloud to obtain a suitable plane (e.g., wall, ceiling, and floor for an indoor scene). To reduce the computational cost of labeling a large number of point clouds, 3-D patches were first extracted using an octree-based method from the point cloud and treated as operating units when labeling them. Based on data quality and density, a patch size of 5 m $\times$ 5 m was adopted.

During the training phase, a patch-based point cloud annotated learning framework [11] was applied to use context information to generate classification results that are better than the results generated by local independent classifiers. The entire point cloud was labeled by the trained model into four categories of wall, ceiling, floor, and others. Then, the labeled planes (points with the same label) were moved to the line structure extraction step. In the proposed method, discrimination between the planes with the same label is not required.

B. Line Structure Extraction on 3-D Point Cloud

To reduce the impact of different qualities and densities of the obtained point cloud data on the registration results, the line structures extracted from the point cloud data is used for registration.

Based on labeling results, a line extraction step was performed on each single labeled plane. First, the normal vector, n_l, of every single point, p_i was calculated as a small facet normal, consisting of a few surrounding points. Then, the tangent plane, T_{p_i}, of each point, p_i was calculated. The tangent plane, T_{p_i}, of each point, p_i, is defined as follows:

$$T_{p_i} = (o_i, n_l) \tag{1}$$

where o_i is the centroid of the small facet used to calculate the normal vector. In 3-D space, the Euclidean distance from any point, p_j, to tangent plane, T_{p_i}, is calculated as follows:

$$\text{dist}(p_j, T_{p_i}) = |(p_j - o_i) \cdot n_l|. \tag{2}$$

The best fitting plane for the set of K neighborhoods of p_i: $B_k(p_i)$ is obtained by solving the following equation:

$$\underset{T_{p_i}}{\text{argmin}} \sum_{p_j \in B_k(p_i)} \text{dist}(p_j, T_{p_i})^2. \tag{3}$$

When all tangent planes, T_{p_i}, for all p_i were calculated, the whole point cloud were divided into small pieces using an improved region growing method. The original region growing method locates as large a plane as possible. In our method, the size of a plane is limited using a parameter, R_{seed}. A point, p_i, was randomly selected as a seed point to create a new facet, $f_i = (\{K_i^m\}, x_i, \vec{T}_i)$, where $\vec{T}_i$ is the unit normal vector of T_{p_i}. For the rest of the point cloud, point p_j was added (or not added) to facet f_i, depending on whether the following three conditions were satisfied.

1) The angle between $\vec{T}_i$ and $\vec{T}_j$ did not exceed the threshold, θ.
2) The distance between p_j and p_i did not exceed R_{seed}.
3) The orthogonal distance from p_j to f_i is less than $\sigma/2$.

When no more points, p_j, could be added to facet, f_i, another point, p_k, was chosen as the seed point, and the search to find facet, f_k, continued until most of the points (80% in this letter) were distributed among the different facets.

Our previous method [12] was improved upon to make it more suitable for indoor point cloud data. Here, we increased the facet size (R_{seed} mentioned above) to: 1) reduce the number of lines in the internal plane and maintain as long a border line as possible; 2) decrease the angle θ between two tangent planes to separate different tangent planes better; and 3) generate a continuous head-to-tail straight line to approximate the edge of the curve structure. To obtain a better line result, we first extract the boundary points of each facet, f_i. Then, to reduce repeated boundary points, we define a facet, F_i, that contains adjacent coplanar facets. Then group boundary points into a cylinder rather than directly group boundary points into line segments. The final step is to obtain a satisfactory line segment from one cylinder using a least median of squares method.

C. Line-Based Point Cloud Integration

Given data for the two point clouds, P and Q, our goal was to find a rigid body transformation, τ, to minimize the distance from $(\tau(P))$ to Q. The rigid body transformation was further

decomposed into a rotation transformation, R, and a translation transformation, T, according to the following equation:

$$\tau(P) = R(Q) + T \tag{4}$$

where R is a 3×3 matrix and T is a 3-D translation vector. The distance function adopts the nearest point principle as follows:

$$E(R,T) = \min_{R,T} \sum_{p_i \in P} ||q_i - (R_{p_i} + T)||^2 \tag{5}$$

where $q_i \in Q$ is the nearest point in Q to the point, p_i after the transformation. Considering that the number of overlapping points is limited, the number of common points (NCP) was chosen as the distance function.

Given a threshold, ϵ, NCP (calculated as follows) is the number of points of the two point clouds whose closet distance is less than ϵ:

$$\begin{aligned}&\mathrm{NCP}(R,T)\\ &= |\{q_i | q_i \in Q \cap \exists p_j \in P \rightarrow ||q_i - (R_{p_j} + T)|| \le \epsilon|.\end{aligned} \tag{6}$$

The target function, defined as finding the R and T that maximize NCP, is as follows:

$$E_{\mathrm{NCP}}(R,T) = \min_{R,T} \mathrm{NCP}(R,T). \tag{7}$$

Considering the quality of the data used, we chose ϵ equals to 15 cm in this letter. Point density between indoor and outdoor point cloud data is different but the density inside a point cloud is relatively uniform. Occlusions in the point cloud decrease the NCP value but the occlusions have the same effect on the NCP value for both indoor and outdoor data.

Most of the door and window (wall opening) structures are quadrilateral structures. Thus, using the above line structure extraction method, a line segment on a wall was extracted, and the potential wall opening structures were extracted using the k-means method. Two lines are grouped if they meet any of the following conditions.

1) The angle between the two lines is smaller than θ, and the shortest distance between the end points of two lines is smaller than d.
2) The angle between the two lines is larger than θ and the longest distance between the endpoints of two lines is less than the sum of the lengths of the two lines.

In this letter, θ and d are set to be 45° and 15 cm, respectively. For wall opening structures, a rigid body transformation is determined from four points. Considering that four edge points are found in each wall opening structure, each of the two-different wall opening structures were matched in a brute force manner. Then, the singular value decomposition (SVD) method was used to find the only transformation matrix. The outdoor point cloud was used as the reference point cloud and the indoor point cloud as the registration point cloud. For each obtained transformation matrix, the NCP values of the converted indoor and outdoor point clouds were calculated, and the optimal matching relationship was selected. In this stage, a coarse registration is obtained because the indoor and outdoor data are not exactly the same data. The ICP-based method [13] fine tunes the coarse registration results for a better result using the structures found in both indoor and outdoor data.

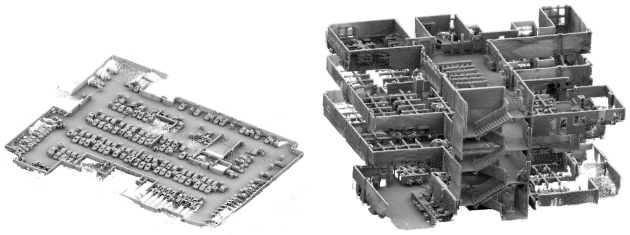

(a) (b)

Fig. 3. Indoor mapping results. (a) Underground garage mapping results. (b) Multifloor mapping results.

TABLE I
ACCURACY OF OUR POINT CLOUD MODEL

Scene	Position	Ground truth (cm)	Measured distance (cm)	Accuracy (%)	Average (%)	Standard deviation (cm)
Underground garage ($87\times77m^2$)	W_a-W_b	4276.77	4271.03	0.13	0.14	9.02
	W_a-W_d	5400.03	5385.77	0.32		
	W_b-W_d	6149.03	6148.27	0.03		
	W_a-W_c	7508.00	7501.73	0.08		
Four-floor Building ($24\times27m^2$)	$FLOOR_1$	1681.04	1686.83	0.45	0.33	5.23
	$FLOOR_2$	1619.25	1618.75	0.20		
	$FLOOR_3$	1789.59	1793.67	0.26		
	$FLOOR_4$	1853.84	1845.86	0.41		

IV. EXPERIMENTS AND RESULTS

A. Indoor Point Clouds Results

1) Accuracy: For analysis, mapping accuracy results were given based on the following two indoor scenes: 1) a single-floor underground garage [Fig. 3(a)], which is relatively empty and with fewer interior objects other than vehicles and 2) a multifloor office building [Fig. 3(b)], which is narrow, complex, and with many pedestrians.

a) Single-floor underground garage: Highly reflective reference points were stuck to four walls (W_a, W_b, W_c, and W_d), with each wall having four reference points. Then a Lecia Viva TS11 total station was used three times to measure the distance from one wall to the other three walls. The three measurements were averaged and considered as ground truth.

b) Multi-floor office building: For this scene, because of serious occlusion, it was inconvenient to use a total station to measure corresponding points at a long distance. A Riegl VZ 1000 TLS [14], which has an error range of millimeters, was first used to scan indoor scenes and measure the distance between two specified points in a point cloud data as a ground truth. Then, from the backpacked point cloud data, two corresponding points were selected and calculated the distance between them. To reduce the errors in the selection of the corresponding points, 20 groups of target points were randomly selected for calculation.

As shown in Table I, the averaged relative accuracies of the garage and the four-floor building are about 0.14% and 0.33%, respectively. The standard deviations of the parking garage and the four-floor building are 9.02 and 5.23 cm, respectively.

2) Precision: To access mapping precision, the RANSAC method was first used to fit the floor and wall planes in the point cloud model. Then, the average standard deviation of the distance from points on the plane to points on the fit plane was calculated. To reduce errors caused by plane fitting, several groups of floor data within a small rectangle were randomly sampled to calculate the weighted average of the

TABLE II
PRECISION OF OUR POINT CLOUD MODEL

Average standard deviation	Underground garage	Office building
Vertical	1.71cm	1.27cm
Planimetric	4.93cm	3.86cm

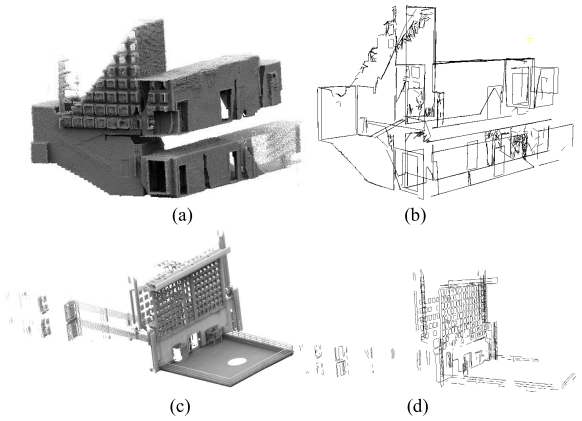

Fig. 4. Line extraction results. (a) Indoor point cloud. (b) Line extraction result of (a). (c). Outdoor TLS point cloud. (d) Line extraction result of (c).

precision of each plane to describe the vertical precision of the mapping result. Similarly, data on a vertical wall within a small area were selected to assess planimetric precision. We chose 5 m × 5 m rectangles about every 10–15 m for the floor, and 3 m × 3 m (according to real wall height) rectangular for the flat wall.

For the underground garage scene, to calculate vertical and planimetric precision, ten small areas of ground or ceiling data and ten small areas of wall or cylinder data were selected, respectively. The average vertical and planimetric standard deviations are about 1.71 and 4.93 cm, respectively (see Table II). For multifloor data, 12 planes in each floor were selected to calculate the local precisions. The average vertical and planimetric standard deviations are about 1.27 and 3.86 cm, respectively (see Table II). The vertical and planimetric local precisions in different indoor scenes indicate our backpacked system provides centimeter-level mapping precision. Larger average planimetric standard deviations are due to significant roll and pitch of the system during movement.

B. Line Structure Extraction

In this experiment, the upgraded backpacked 3-D laser scanning system and a Riegl VZ-1000 TLS were used to obtain indoor [Fig. 4(a)] and outdoor point cloud data [Fig. 4(c)], respectively. Thus, the acquired indoor data are centimeter-level precision and the acquired outdoor data are millimeter-level precision, respectively. The indoor scene consists of two levels of corridors. Only the end of the corridor is connected to the outdoor scene. In all experiments, according to the quality of point cloud data and tests, the R_{seed} was set at 3.5 m, and σ was set at 0.2 m. Line structure extraction results of the indoor and outdoor point cloud data, obtained by the method mentioned in Section III-B, are shown in Fig. 4(b) and (d), respectively.

As shown in Fig. 4, the line structures extracted from the original point cloud data is too complex and noisy. It is difficult to match the line structures from the backpacked and TLS point cloud sources directly based on this line results.

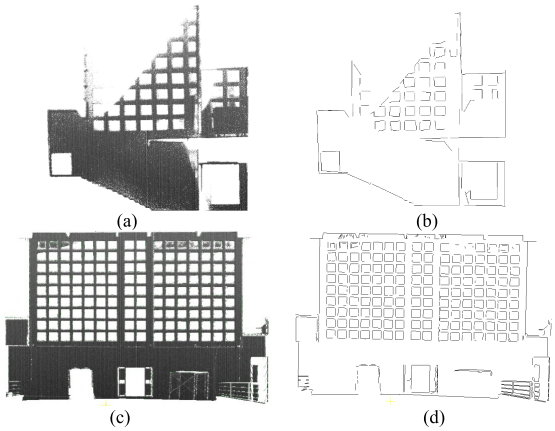

Fig. 5. Line extraction results of wall area. (a) Indoor backpacked point cloud. (b) Line extraction result of (a). (c) Outdoor TLS point cloud. (d) Line extraction result of (c).

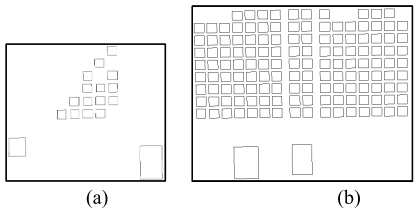

Fig. 6. Wall openings. (a) Indoor backpacked data. (b) Outdoor TLS data.

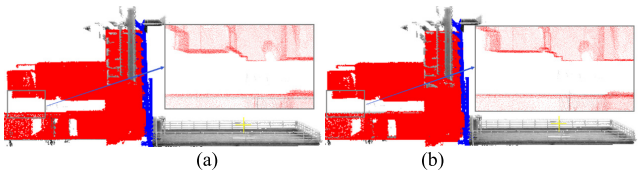

Fig. 7. Registration results. Blue represents outdoor data and red represents indoor data. (a) Coarse registration. (b) Fine registration.

Therefore, the wall point cloud data were first labeled out, and 3-D lines were extracted only on the wall plane (Fig. 5).

C. Registration Results

Based on wall line structures, the potential window and door structures were detected using a k-means clustering method first, and then regularized them based on the assumption that they are quadrilaterals (Fig. 6).

There are not very many matched structures between two point cloud data sets. (In Fig. 6, there are 17 rectangles on the left and 140 on the right.) Thus, a brute force manner was adopted to match structures, and the SVD method was adopted to calculate the transformation matrix for every single match. The computational time to find the best transformation matrix was 623 s. (Our code runs on windows 10, CPU Intel Core i5-4460 at 3.20 GHz, 12-GB RAM.)

Based on coarse registration results, refinement of the results was achieved by an ICP-based method [13]. To quantify our registration results, the rms distance between corresponding points of outdoor and indoor point clouds (after registration) were used. For a pair of points $\{p, q\}$ ($\forall p \in P, \forall q \in Q$) in the data of two point clouds, the pair $\{p, q\}$ are the common points if they satisfy the following two conditions: 1) point, p, is the closet one in P to point q or vice versa and 2) the distance between point, p, and point, q, is less than a predefined

TABLE III
REGISTRATION DISTANCE

	Coarse registration	Fine registration
Min distance(cm)	7.6777e-04	2.2057e-05
Max distance(cm)	0.3584	0.2088
Ave distance(cm)	0.1632	0.0485

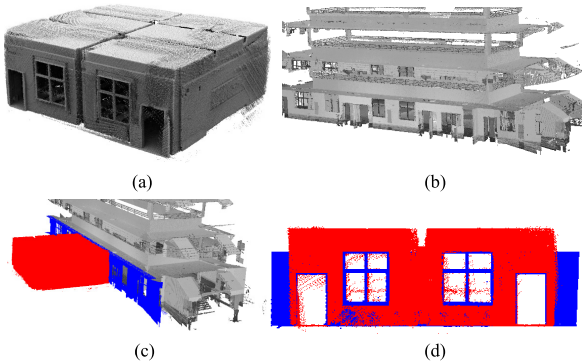

Fig. 8. Room scene registration results. Blue represents outdoor data and red represents indoor data. (a) Indoor backpacked point cloud. (b) Outdoor TLS data. (c) Registration results. (d) Another view of registration results.

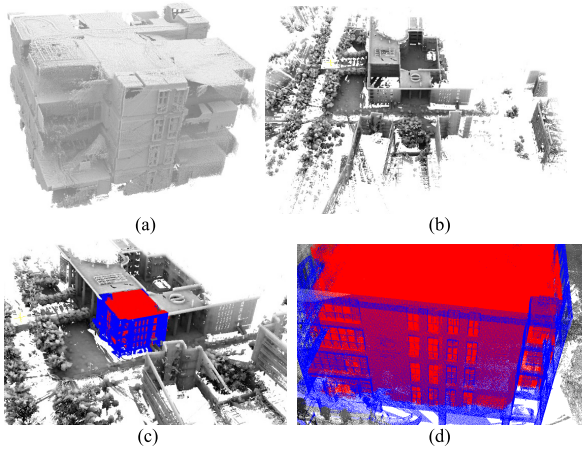

Fig. 9. Building scene registration results. Blue represents outdoor data and red represents indoor data. (a) Indoor backpacked point cloud. (b) Outdoor TLS data. (c) Registration results. (d) Another view of registration results.

threshold (set at 10 cm in this letter). The rms values for coarse and fine registration are 7.54 and 6.81 cm, respectively, which indicates the effects of the refinement process in our method.

The 4PCS and super-4PCS methods were used to test this scene too. These two methods use the point cloud's geometric features the affine invariance of the planar quadrilateral to find the corresponding points. In this scene, to register the indoor and outdoor point cloud data, both methods try to find the points at the top of the corridor. However, they fall into a local optimum and cannot register the scene correctly.

To further test the accuracy of our method, the ceiling of the corridor in the outdoor scene data were extracted and fit the ceiling to obtain a plane (Fig. 7). In Fig. 7, the blue point cloud is outdoor data, red point cloud is indoor data, and the gray point cloud is outdoor data that does not involve registration. Then, to calculate the distance from the ceiling of the corridor to the fit plane in the outdoor scene data, the ceiling at the same location in the indoor scene data were selected. Detailed numerical values are shown in Table III. The average distances for the two planes of coarse and fine registrations are 0.1632 and 0.0485 cm, respectively.

Another two test scene results are shown in Figs. 8 and 9. To obtain the indoor [Figs. 8(a) and 9(a)] and outdoor point cloud data [Figs. 8(b) and 9(b)], the upgraded backpacked laser scanning system and a Riegl VZ-1000 TLS were used, respectively. The fine registration results for indoor and outdoor are given in Figs. 8(c) and (d) and 9(c) and(d), respectively. As seen in Figs. 8(c) and (d) and 9(c) and (d), the proposed method deals with the indoor and outdoor integration for point cloud data with different quality and scenes with different structure.

V. CONCLUSION

This letter presented an indoor and outdoor integration method using backpacked laser scanning point cloud data and TLS point cloud Data. Although the proposed method uses the above two types of data, in practice, this method can be adapted to the point cloud data obtained by different sensors. However, this method requires the buildings to be registered, have coincident parts, and contain the quadrilateral structure of windows and doors (not including cylinders and curved shapes). To locate potential indoor-outdoor overlapping areas, a semantic labeling method was used to label wall areas. To register two point clouds with different data qualities, a 3-D line structure was extracted directly from the point clouds for further registration. The results show that our method is promising for use with point cloud data of different qualities.

REFERENCES

[1] D. Zai *et al.*, "Pairwise registration of TLS point clouds using covariance descriptors and a non-cooperative game," *ISPRS J. Photogramm. Remote Sens.*, vol. 134, pp. 15–29, Dec. 2017.
[2] T. Koch, M. Körner, and F. Fraundorfer, "Automatic alignment of indoor and outdoor building models using 3D line segments," in *Proc. IEEE Conf. Comput. Vis. Pattern Recognit. Workshops*, Jun./Jul. 2016, pp. 689–697.
[3] J. J. Koenderink and A. J. van Doorn, "Affine structure from motion," *J. Opt. Soc. Amer. A*, vol. 8, no. 2, pp. 377–385, 1991.
[4] A. Cohen, J. L. Schnberger, P. Speciale, and T. Sattler, "Indoor-outdoor 3D reconstruction alignment," in *Proc. Eur. Conf. Comput. Vis.*, 2016, pp. 285–300.
[5] N. J. Mitra, N. Mellado, and D. Aiger, "Super 4PCS fast global pointcloud registration via smart indexing," *Comput. Graph. Forum*, vol. 33, no. 5, pp. 205–215, Aug. 2014.
[6] D. Aiger, N. J. Mitra, and D. Cohen-Or, "4-points congruent sets for robust pairwise surface registration," *ACM Trans. Graph.*, vol. 27, no. 3, 2008, Art. no. 85.
[7] C. Wen, S. Pan, C. Wang, and J. Li, "An indoor backpack system for 2-D and 3-D mapping of building interiors," *IEEE Geosci. Remote Sens. Lett.*, vol. 13, no. 7, pp. 992–996, Jul. 2016.
[8] C. Wang *et al.*, "Semantic line framework-based indoor building modeling using backpacked laser scanning point cloud," *ISPRS J. Photogramm. Remote Sens.*, to be published, doi: 10.1016/j.isprsjprs.2018.03.025.
[9] J. Zhang and S. Singh, "LOAM: Lidar odometry and mapping in real-time," in *Proc. Robot., Sci. Syst. Conf.*, 2014, pp. 1–9.
[10] R. Kümmerle, G. Grisetti, H. Strasdat, K. Konolige, and W. Burgard, "G^2o: A general framework for graph optimization," in *Proc. IEEE Int. Conf. Robot. Automat.*, May 2011, pp. 3607–3613.
[11] H. Luo *et al.*, "Patch-based semantic labeling of road scene using colorized mobile LiDAR point clouds," *IEEE Trans. Intell. Transp. Syst.*, vol. 17, no. 5, pp. 1286–1297, May 2016.
[12] Y. Lin *et al.*, "Line segment extraction for large scale unorganized point clouds," *ISPRS J. Photogramm. Remote Sens.*, vol. 102, pp. 172–183, Apr. 2015.
[13] S. Rusinkiewicz and M. Levoy, "Efficient variants of the ICP algorithm," in *Proc. 3rd Int. Conf. 3-D Digit. Imag. Modeling*, May/Jun. 2001, pp. 145–152.
[14] *DataSheet_VZ-1000*. Accessed: Jun. 14, 2017. [Online]. Available: http://www.riegl.com/uploads/tx_pxpriegldownloads/DataSheet_VZ-1000_2017-06-14.pdf